Dynamics of colloidal particles in ice

Melissa Spannuth,[1,a)] S. G. J. Mochrie,[2] S. S. L. Peppin,[3] and J. S. Wettlaufer[1,2,4,5]
[1]*Department of Geology and Geophysics, Yale University, New Haven, Connecticut 06520, USA*
[2]*Department of Physics, Yale University, New Haven, Connecticut 06520, USA*
[3]*OCCAM, Mathematical Institute, University of Oxford, Oxford OX1 3LB, United Kingdom*
[4]*Program in Applied Mathematics, Yale University, New Haven, Connecticut 06520, USA*
[5]*NORDITA, Roslagstullsbacken 23, SE-10691 Stockholm, Sweden*

(Received 25 July 2011; accepted 14 November 2011; published online 13 December 2011)

We use x-ray photon correlation spectroscopy (XPCS) to probe the dynamics of colloidal particles in polycrystalline ice. During freezing, the dendritic ice morphology and rejection of particles from the ice created regions of high particle density, where some of the colloids were forced into contact and formed disordered aggregates. The particles in these high density regions underwent ballistic motion, with a characteristic velocity that increased with temperature. This ballistic motion is coupled with both stretched and compressed exponential decays of the intensity autocorrelation function. We suggest that this behavior could result from ice grain boundary migration. © *2011 American Institute of Physics*. [doi:10.1063/1.3665927]

I. INTRODUCTION

Solidification of the solvent phase of a colloidal suspension occurs in a wide variety of natural and technological settings. Owing to the rapidly expanding domain of materials applications, and relatively simple and inexpensive processing methods, a variety of solidification procedures are receiving intense theoretical and experimental study.[1] Under a wide range of conditions, as the solvent freezes the interface between the liquid and solid solvent ramifies, guiding the particles into a variety of macroscopic morphologies. At the lowest freezing velocities all of the particles are rejected and pushed ahead of a planar solid-liquid interface, while at higher velocities a dendritic solid-liquid interface aligns the particles into microporous structures, or solid lenses segregate the particles into periodic layers.[2,3] At the highest growth rates the solid engulfs the particles individually. These various regimes have many applications including purifying water,[4] creating tissue scaffolds,[5] understanding ground freezing,[6] and building composite materials.[7] The progression through the various regimes and their properties are fundamentally important, but involve a hierarchy of poorly understood cooperative phenomena. One of the factors limiting understanding is a lack of experiments revealing the particle behavior at the smallest length scales. Here, we provide the first investigation of particle dynamics within frozen colloidal suspensions.

We used x-ray photon correlation spectroscopy (XPCS) to examine the dynamic behavior of spherical silica colloids encased in ice. During freezing, the particles were forced into high particle density regions between ice grains where the attractive van der Waal's interactions caused irreversible aggregation.[8] The polycrystalline ice then coarsened, carrying the particle aggregates as well as any unaggregated particles along in the migrating grain boundaries. We measured the particle motion with XPCS and found a unique type of behavior.

The scattering revealed ballistic particle dynamics combined with a non-exponential decay of the intensity autocorrelation function (ACF). This combination with a compressed exponential decay is commonly observed in light scattering from soft materials. Uniquely in our experiments, the decay is *slower* than exponential at *small* scattering vectors and *faster* than exponential at *large* scattering vectors. While ballistic dynamics combined with a stretched exponential have been reported previously in one other system, ours is evidently the first observation of a transition from stretched to compressed exponential behavior with increasing scattering vector. The measured characteristic velocity of the particles in our experiments agrees with the expected grain boundary velocities, suggesting that grain boundary migration is the ultimate source of the ballistic motion. The unusual form of the ACF most likely results from the deformation of the collection of particles within the grain boundary and we suggest several possibilities. Further experimental and theoretical study of this type of system will not only clarify the behavior of particles in frozen colloidal suspensions, but also provide insight into a wide range of soft materials.

II. MATERIAL AND METHODS

Four independent samples of colloidal silica spheres (Polysciences, Inc.) dispersed in deionized water were solidified, and the composite material interrogated via x-ray scattering. The particle radius $R = 32$ nm, polydispersity $z = 18\%$, and initial unfrozen particle volume fraction $\phi \approx 0.02$ were determined from small angle x-ray scattering (SAXS) and scanning electron micrographs.[8] The samples were contained in an approximately 400 μm thick, temperature-controlled sample chamber that produced a cylindrical isothermal region 2 mm in diameter.[8] Observations were made at five locations within the isothermal region of the samples.

[a)]Present address: Department of Chemical and Biomolecular Engineering, University of Houston, Houston, Texas 77204, USA. Electronic mail: melissa.spannuth@gmail.com.

 © 2011 American Institute of Physics

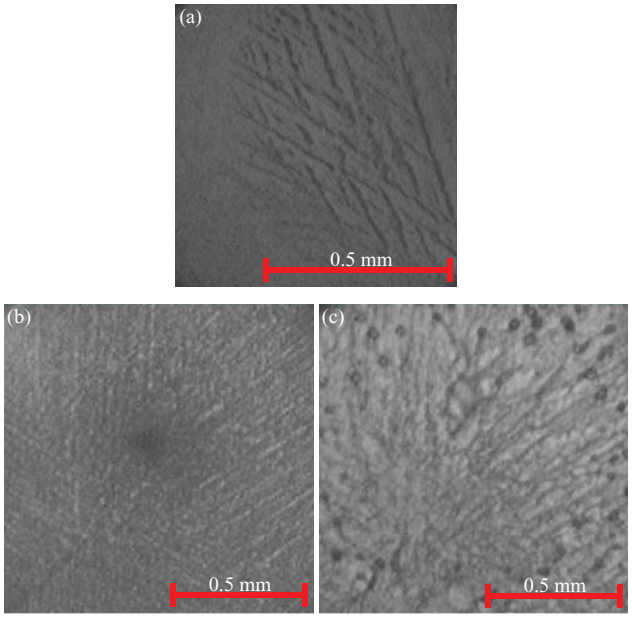

FIG. 1. Images from video microscopy of freezing colloidal suspensions. Image (a) shows ice dendrites during growth and rejected particles (dark linear features) in a sample with 284-nm-diameter silica particles. Images (b) and (c) show the time evolution over 25 h in a sample of 64-nm-diameter particles. The dark regions are areas of high particle density, which appear to move with the grain boundaries over time (the dark circles near the edges of the image are air bubbles). The image in (b) was acquired at $T = -2.5\,^{\circ}\mathrm{C}$ shortly after freezing, and the image in (c) was acquired at $T = 0\,^{\circ}\mathrm{C}$ shortly before melting.

The solvent was frozen by lowering the temperature at a rate of about 1 °C/s. Ice nucleation usually occurred between temperatures $T = -20\,^{\circ}\mathrm{C}$ and $-30\,^{\circ}\mathrm{C}$. Therefore, the water in all samples was highly supercooled when ice growth began, likely resulting in an unstable solidification front and a cellular or dendritic ice growth morphology.[2,9,10] Indeed, when we observed samples freezing under similar conditions with video microscopy the ice growth was dendritic[8] as illustrated in Fig. 1(a). The colloidal particles were rejected into the regions between relatively pure ice dendrites resulting in linear regions of high particle density tens of μm wide separated by regions of low particle density of approximately the same width[8] (Fig. 1(b)). Small-angle x-ray scattering revealed that the particles in the high density regions were touching and probably close packed, though the distribution of interparticle distances was broader than expected for a colloidal fluid or glass at high volume fraction.[8] The close packing likely resulted in particles binding together into amorphous clusters.[8]

After freezing at low temperature, T was increased to near the melting temperature, at which point XPCS data collection commenced. We collected sets of images of the scattered x-ray intensity $I(\mathbf{q}, t)$ at various scattering vectors $\mathbf{q}$ and times t for T increasing from $-2\,^{\circ}\mathrm{C}$ to $0\,^{\circ}\mathrm{C}$ in steps as small as $0.05\,^{\circ}\mathrm{C}$. While T increased, the particles moved, as demonstrated by the microscopy image in Fig. 1(c) taken 25 h after freezing. This motion resembles the motion of ice grain boundaries observed in samples without particles. The XPCS data measure particle motion during this period. Because sample age necessarily increased along with T, any effects of aging are combined with the effects of increasing T.

The x-ray scattering was performed at sector 8-ID-I of the Advanced Photon Source.[11] The beam size was 20 μm $\times$ 20 μm, ensuring that the illuminated volume of the sample contained millions of particles. Due to the large density contrast between water and silica, the scattered signal is dominated by scattering from the particles. Occasionally in the raw intensity images, we observed specular reflections from air bubbles or grain boundary grooves intersecting the sample chamber walls.[12] These were masked out before further analysis. Thus, we expect that the observed dynamics are due solely to the motion of particles.

We used the multispeckle XPCS method to obtain the intensity autocorrelation function $g_2(q, \tau) = \langle I(q, t) I(q, t + \tau)\rangle / \langle I(q)\rangle^2$ from the azimuthally averaged intensity $I(q, t)$. Here $\langle \cdots \rangle$ represents an ensemble average over the detector pixels and τ is the delay time between the two frames for which the correlation is calculated. In addition to ensemble averaging, we used a multi-tau scheme with four delays per level to improve the ACF signal-to-noise ratio. The intensity ACF contains information about the particle dynamics through the shape and rate of its decay.[13] The length-scale of the dynamics probed is related to q; by using x-rays, we accessed length-scales comparable to the size of the individual particles.

III. RESULTS

Figure 2 shows several ACFs at $q \approx 0.1\ \mathrm{nm}^{-1}$ (near the peak in the static scattered intensity) for a sample at four temperatures from $T = -0.60\,^{\circ}\mathrm{C}$ to $T = -0.30\,^{\circ}\mathrm{C}$. These data represent the typical forms of $g_2(q, \tau)$ observed: either a single decay or two decays in which the second is extremely stretched and of small amplitude. Although we have only shown ACFs for a single representative q, the form of the ACF is always the same at all q for a particular position in a given sample at a certain T. For data with two decays, we are only concerned with the decay at small τ. As the temperature

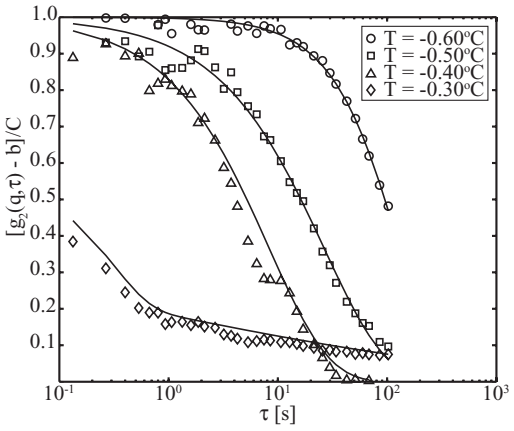

FIG. 2. Adjusted intensity ACFs $[g_2(q, \tau) - b]/C$ versus delay time τ from sample 1 (of four) at $T = -0.60\,^{\circ}\mathrm{C}$ (circles), $T = -0.50\,^{\circ}\mathrm{C}$ (squares), $T = -0.40\,^{\circ}\mathrm{C}$ (triangles), and $T = -0.30\,^{\circ}\mathrm{C}$ (diamonds) with the corresponding stretched or compressed exponential fits (solid curves).

increases, the decay rate also increases, so that the decay time becomes shorter.

In order to quantify the changes in decay time and shape, we fit each $g_2(q, \tau)$ to a Kohlrausch-Williams-Watts (KWW) expression[14] or a combination of two KWW expressions. Single decays were fit with $g_2(q, \tau) = b + C\exp[-2(\Gamma\tau)^{\alpha}]$, where the fitting parameters are the baseline b, the contrast C, the decay rate Γ, and the stretching (<1) or compressing (>1) exponent α. Similarly, we fit double decays with $g_2(q,\tau) = 1 + C\{(1-\beta)\exp[-(\Gamma_F\tau)^{\alpha_F}] + \beta\exp[-(\Gamma_S\tau)^{\alpha_S}]\}^2$, where C, Γ, and α are as above. The "partition coefficient" β describes the relative strength of the two exponential decays, and the subscripts denote the first (F) or second (S) decay.

As illustrated by the solid curves in Fig. 2, these functions are consistent with the data. Most of the data from all five positions in each of the four samples could be quantified in this way, but some were too noisy or had features that did not fit into this analysis framework. Although we primarily observed particles in the high density regions between ice grains, the particle distribution was clearly heterogeneous and constantly evolving. We ascribe the occasional appearance of abnormal ACFs to the spatial heterogeneity produced by the inherently stochastic nature of the ice nucleation process, the unstable ice growth morphology, and the process of ice crystal coarsening in the polycrystalline ice.

Both Γ and α resulting from these fits vary with q. Figure 3(a) shows examples of Γ versus q for a sample at several temperatures between $T = -1.60\,^{\circ}$C and $T = -0.70\,^{\circ}$C, each of which increase linearly with q. In some cases, a linear extrapolation of Γ to $q = 0$ nm^{-1} would not pass through the origin. This simply indicates the presence of a q-independent component to the relaxation, such as the rate of very large displacement events for which the entire sample within the scattering volume is exchanged.[15]

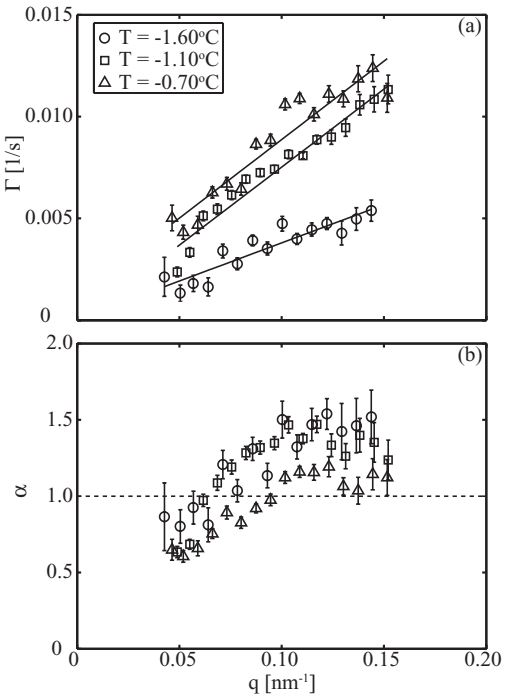

FIG. 3. In (a), examples of decay rate Γ are plotted versus scattering vector q from sample 1 at $T = -1.60\,^{\circ}$C (circles), $T = -1.10\,^{\circ}$C (squares), and $T = -0.70\,^{\circ}$C (triangles) with their respective linear fits (solid lines). In (b), the corresponding exponents α are plotted versus q.

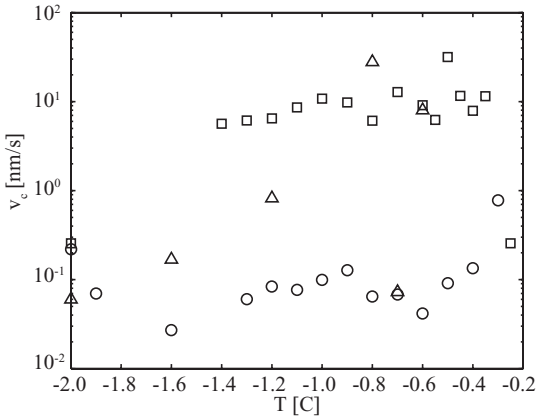

FIG. 4. The characteristic velocity v_c versus temperature T for one position in each of sample 1 (circles), sample 2 (squares), and sample 4 (triangles).

Figure 3(b) shows examples of α versus q from the same data as in Fig. 3(a). In all cases, α is between 0.5 and 1 at low q and increases to between 1 and about 1.5 at higher q, leveling off for $q \gtrsim 0.12$ nm^{-1}. (For comparison, the measured structure factor from SAXS (Ref. 8) has a peak at $q = 0.123$ nm^{-1} and the particle size corresponds to $q = \pi/32$ nm $= 0.0981$ nm^{-1}.)

This behavior of Γ and α indicates ballistic (as opposed to diffusive) particle dynamics and can be described with a distribution of particle velocities similar to a Lévy stable distribution, which has a power law tail.[16] The characteristic velocity v_c of the particles is the slope of a linear fit to Γ versus q (solid lines in Fig. 3(a)). We have fit Γ from the data analyzed in this framework to find that v_c generally increases with increasing temperature as shown in Fig. 4. The orders of magnitude difference between the curves can be ascribed to the variability introduced by the freezing process.

Finally, we note that the fitted contrast is always less than unity, indicating the possibility of particle dynamics at time scales shorter than those accessible in the present experiments. Alternately, these values of C could reflect instrumental effects that result in a Siegert factor less than unity. We estimated the Siegert factor from ACFs at very low temperature ($T < -20\,^{\circ}$C) to be about 0.6. However, this value is highly uncertain because the static ACFs have rather large error bars. While the fitted contrast typically falls below the Siegert factor estimated in this manner, suggesting the presence of fast dynamics, the large uncertainty in the estimated Siegert factor means the discrepancy may be negligible within our error bounds. In addition, XPCS experiments accessing slightly shorter delay times showed no indication of fast dynamics (all ACFs appeared static). Future experiments should include both more accurate measurements of the Siegert factor as well as dynamic measurements at very short delay times in order to detect the presence of fast dynamics, which may indicate caged motion of the particles.

IV. DISCUSSION

While ballistic dynamics combined with a compressed exponential decay of $g_2(q, \tau)$ has become a common observation,[16–19] the combination of ballistic dynamics with a stretched exponential decay is rare[15] and a *transition* from a *stretched* to *compressed* exponential decay with increasing scattering vector has not been reported previously. Either stretched or compressed decays could result from a continuous time random walk in which the size of the steps performed by the scatterers is distributed according to the Lévy alpha-stable distribution. This explanation is not specific to a particular material or system, and ascribing a physical origin to the necessary step size distribution can be difficult. For colloidal gels, considering the relaxation of stress dipoles induced during disturbances to the material (e.g., shear or loading into a container) produces the values of $\alpha \approx 1.5$ obtained in many experiments.[18,20] However, few other systems exhibiting this type of behavior have such a complete description.

In our experiments the high-particle-density regions, which dominate the scattering, contained colloidal aggregates that formed when the solutions froze. We argue here that grain boundary motion arising from coarsening of the polycrystalline ice exerts forces on these aggregates resulting in the observed dynamic scattering. From SAXS performed simultaneously with XPCS, we know that the particles in the high density regions were close-packed and touching.[8] The forces associated with particle rejection from the ice front during freezing are sufficient to overcome the electrostatic repulsion between the particles and bring them into contact.[21] Once in contact, the van der Waal's attraction between the particles caused them to bind to each other forming an amorphous colloidal solid. The attractive energy for these particles is estimated to be 9×10^{-20} J, or about $24 k_B T$ at $T = 273$ K, so thermal energy alone would be insufficient to completely disperse the aggregates on experimental time-scales. Indeed, using video microscopy we observed high-particle-density aggregates up to hundreds μm in size sedimenting through the melted samples. SAXS measurements indicated that about half of the particles initially in the solution sedimented.[8] Thus, the grain boundaries between ice crystals probably contained a mixture of aggregates and single particles.

In order for the polycrystalline ice to coarsen, the aggregates and particles in the grain boundaries must deform under stresses transmitted from the ice crystals. We estimate the strength of these forces from the pressure ΔP driving the ice crystal coarsening: $\Delta P = \gamma_{gb}\kappa$, where γ_{gb} is the surface free energy of the grain boundary and κ is the curvature of the boundary.[22] Taking $\gamma_{gb} = 0.033$ J/m^2, which is the value for an ice-water interface (interstices between the particles should be water-filled at the T studied due to curvature-induced depression of the melting temperature), and $\kappa = 1/R_c = 10^4$ m^{-1}, where $R_c = 100\,\mu$m is an estimate of the ice grain boundary radius of curvature determined from the grain size in microscopy images. This gives $\Delta P = 330$ N/m^2, which is distributed across the particles adjacent to the ice. Assuming that the pressure is distributed across about half the surface of a $10\,\mu$m radius aggregate, the total force on the aggregate is about 2.1×10^{-7} N. At $\phi = 0.6$, this amounts to a force per particle on the surface F_p of about 1.2×10^{-12} N. In order for the aggregate to deform, we assume that a particle must move a distance equal to one particle diameter (64 nm). The work performed by F_p in moving a particle this distance is about 8×10^{-20} J, nearly the van der Waal's energy binding the particles together (9×10^{-20} J). Therefore, grain boundary motion induced by coarsening of the polycrystalline ice could deform the colloidal aggregates.

Although other stress sources are possible, grain boundary motion from coarsening produces characteristic velocities of the correct order of magnitude. The grain boundary velocity is given by $v_{gb} = M\gamma_{gb}\kappa$, where M is the grain boundary mobility. The product $M\gamma_{gb}$ for ice at $T = -5^\circ$C ranges from about 10^{-11} to 10^{-14} m^2/s.[23] Thus, for the value of κ given above, v_{gb} could be between 0.1 and 100 nm/s, encompassing the observed range of v_c. Variations in grain size and mobility among the samples can account for the large differences between the characteristic velocities shown in Fig. 4. Grain boundary migration can also produce the increase in the characteristic velocity with temperature through the Arrhenius behavior of the grain boundary mobility.[23] Furthermore, translation of particles within the grain boundary across the entire scattering volume can explain the q-independent component to the decay time, and the magnitude of the grain boundary velocities given above even results in a time scale for particle transport across the beam diameter in agreement with the time estimated from extrapolation of Γ to $q = 0$ nm^{-1}.

Determining how the stresses produced by grain boundary migration would affect the motion of particles in the grain boundaries is challenging; we discuss two complementary scenarios. It is unlikely that the stress resembles the dipolar stress sources proposed to explain compressed exponential decay and ballistic motion.[20] Instead, the very high particle density may cause the colloids to behave more like a granular material[24] so that forces are distributed along force chains.[25] Such a direct transmission of the grain boundary motion would produce ballistic particle motion at about the same rate as the grain boundary was moving. However, the distribution of the force would cause particles to experience stress only sporadically. At larger length scales (low q), there would be a wider range of decay times (smaller α) because the sporadic stress may be greater or less than that required to cause the necessary particle displacement for decorrelation of the intensity ACF. Whereas, at smaller length scales (large q) almost any stress would deform the particles sufficiently for decorrelation and thus there would be a narrower distribution of decay times (larger α). However, the stress is still imposed sporadically leading to a non-negligible possibility of very long waiting times between imposition of sufficient stress, and hence a power law form for the tail of the distribution.

We can connect this type of behavior with prior theoretical work on solidifying colloidal suspensions and self-filtration. In colloidal suspensions near random close packing, the osmotic pressure, and hence the generalized form of the Stokes-Einstein (mutual) diffusivity, diverge as the particle volume fraction approaches random close packing.[2,3,26] Then, the character of diffusive relaxation of particle concentration gradients becomes extremely long ranged such that

very near the divergent limit diffusion becomes effectively "instantaneous." Thus, imposing a force on the close-packed colloids in the grain boundary leads to immediate and long-ranged particle motion, i.e., force chains. Such behavior of the diffusivity can be understood to drive ballistic motion.

V. CONCLUSION

We have used x-ray scattering to study particle-scale dynamics in frozen colloidal suspensions. In applying XPCS to silica particles in ice, we discovered a unique type of particle dynamics that combines ballistic particle motion with an intensity ACF that transitions from a stretched to compressed exponential decay with increasing scattering vector. We have provided a scenario to explain how such behavior could result from grain boundary migration induced by ice crystal coarsening, which provides a framework for more detailed theoretical studies. Such study is warranted given other similar, as yet unexplained results,[15] and more such results are sure to emerge as x-ray scattering is further applied to non-equilibrium soft matter systems.

With a better understanding of how different types of stresses are manifest in particle motion and scattering, XPCS will reveal more detailed information about particle-scale behavior of colloids in freezing suspensions. Future experiments should examine the aging behavior at a fixed temperature, as well as the variation in particle dynamics with sample parameters such as volume fraction and particle size.

ACKNOWLEDGMENTS

We thank S. Narayanan, A. Sandy, and M. Sprung for assistance with the XPCS experiments, and X. Lu, J. Neufeld, E. Thomson, and L. Wilen for useful discussions. M.S. acknowledges the NSF Graduate Research Fellowship for support. S.G.J.M. thanks the NSF for support via DMR-0906697. S.S.L.P. acknowledges support from KAUST Award KUK-C1-013-04. J.S.W. acknowledges support from NSF Grant OPP0440841, the US DoE Grant DE-FG02-05ER15741, and the Wenner-Gren and John Simon Guggenheim Foundations. Use of the Advanced Photon Source was supported by the US DoE under Contract No. DE-AC02-06CH11357.

[1] S. Deville, Adv. Eng. Mater. **10**, 155 (2008).
[2] S. S. L. Peppin, M. G. Worster, and J. S. Wettlaufer, Proc. R. Soc. A **463**, 723 (2007).
[3] S. S. L. Peppin, J. S. Wettlaufer, and M. G. Worster, Phys. Rev. Lett. **100**, 238301 (2008).
[4] G. Gay and M. A. Azouni, Cryst. Growth Des. **2**, 135 (2002).
[5] Q. Fu, M. N. Rahaman, F. Dogan, and B. S. Bal, J. Biomed. Mater. Res. A **86B**, 125 (2008).
[6] J. G. Dash, A. W. Rempel, and J. S. Wettlaufer, Rev. Mod. Phys. **78**, 695 (2006).
[7] G. Wilde and J. H. Perepezko, Mater. Sci. Eng., A **283**, 25 (2000).
[8] M. Spannuth, S. G. J. Mochrie, S. S. L. Peppin, and J. S. Wettlaufer, Phys. Rev. E **83**, 021402 (2011).
[9] A. A. Shibkov, Y. I. Golovin, M. A. Zheltov, A. A. Korolev, and A. A. Leonev, Physica A **319**, 65 (2003).
[10] S. Deville, E. Maire, G. Bernard-Granger, A. Lasalle, A. Bogner, C. Gauthier, J. Leloup, and C. Guizard, Nat. Mater. **8**, 966 (2009).
[11] D. Lumma, L. B. Lurio, S. G. J. Mochrie, and M. Sutton, Rev. Sci. Instrum. **71**, 3274 (2000).
[12] M. Spannuth, "Structure and dynamics in freezing and frozen colloidal suspensions from direct imaging and x-ray scattering," Ph.D. dissertation (Department of Geology and Geophysics, Yale University, 2010).
[13] B. J. Berne and R. Pecora, *Dynamic Light Scattering* (Wiley, New York, 1976).
[14] G. Williams and D. Watts, Trans. Faraday Soc. **66**, 80 (1970).
[15] E. M. Herzig, A. Robert, D. D. van' t Zand, L. Cipelletti, P. N. Pusey, and P. S. Clegg, Phys. Rev. E **79**, 011405 (2009).
[16] L. Cipelletti, L. Ramos, S. Manley, E. Pitard, D. Weitz, E. Pashkovski, and M. Johansson, Faraday Discuss. **123**, 237 (2003).
[17] R. Bandyopadhyay, D. Liang, H. Yardimci, D. A. Sessoms, M. A. Borthwick, S. G. J. Mochrie, J. L. Harden, and R. L. Leheny, Phys. Rev. Lett. **93**, 228302 (2004).
[18] A. Duri and L. Cipelletti, Europhys. Lett. **76**, 972 (2006).
[19] C. Caronna, Y. Chushkin, A. Madsen, and A. Cupane, Phys. Rev. Lett. **100**, 055702 (2008).
[20] J. Bouchaud and E. Pitard, Eur. Phys. J. E **9**, 287 (2002).
[21] A. W. Rempel and M. G. Worster, J. Cryst. Growth **205**, 427 (1999).
[22] J. W. Cahn, Acta Metall. **10**, 789 (1962).
[23] O. B. Nasello, C. L. Di Prinzio, and P. G. Gusmán, Acta Mater. **53**, 4863 (2005).
[24] M. D. Haw, Phys. Rev. Lett. **92**, 185506 (2004).
[25] H. M. Jaeger, S. R. Nagel, and R. P. Behringer, Rev. Mod. Phys. **68**, 1259 (1996).
[26] S. S. L. Peppin, J. A. W. Elliot, and M. G. Worster, J. Fluid Mech. **554**, 147 (2006).